Lattice dynamics in elemental modulated Sb_2Te_3 films

D. Bessas[1,2,3,*], M. Winkler[4], I. Sergueev[5,6], J. D. König[4], H. Böttner[4], R. P. Hermann[1,2]

[1] Jülich Center for Neutron Science JCNS and Peter Grünberg Institut PGI, JARA-FIT, Forschungszentrum Jülich GmbH, D-52425 Jülich, Germany
[2] Faculté des Sciences, Université de Liège, B-4000, Liège, Belgium
[3] Present address: European Synchrotron Radiation Facility, F-38043 Grenoble, France
[4] Fraunhofer Institute for Physical Measurement techniques IPM, Heidenhofstrasse 8, D-79110 Freiburg, Germany
[5] European Synchrotron Radiation Facility, F-38043 Grenoble, France
[6] Present address: Deutsches Elektronen-Synchrotron, D-22607 Hamburg, Germany

Received XXXX, revised XXXX, accepted XXXX
Published online XXXX

Key words: Lattice dynamics, elemental modulated, Sb_2Te_3 films

* Corresponding author: e-mail bessas@esrf.fr

The crystallinity and the lattice dynamics in elemental modulated Sb_2Te_3 films are investigated microscopically using high energy synchrotron radiation diffraction combined with ^{121}Sb nuclear inelastic scattering. The correlation length is found to be finite but less than 100 Å. The element specific density of phonon states is extracted. A comparison with the element specific density of phonon states in bulk Sb_2Te_3 confirms that the main features in the density of phonon states arise from the layered structure. The average speed of sound at 40 K, $1.74(2)$ km/s, is almost the same compared to bulk Sb_2Te_3 at 20 K, $1.78(2)$ km/s. Similarly the change in the acoustic cut-off energy is within the experimental detection limit. Thus, we suggest that the lattice thermal conductivity in elemental modulated Sb_2Te_3 films should not be significantly changed from its bulk value.

1 Introduction Tetradymite chalcogenide compounds usually form anisotropic layered structures [1] with interesting lattice dynamics [2]. It is thus intriguing to study the Density of Phonon States, DPS, on artificially created layered compounds which mimic the natural crystal structures and compare it with reference data on the bulk polycrystalline counterparts.
Sb_2Te_3 crystallises in the tetradymite structure ($R\overline{3}m$, #160) with three quintuple -[Te(I)-Sb-Te(II)-Sb-Te(I)]- stacks forming a unit cell. The parenthetical indices, Te(I) and Te(II) denote two tellurium sites. The easy cleavage of these compounds perpendicular to the c-axis is due to weak van der Waals type binding [3] between quintuple stacks at the Te(I) - Te(I) bond.
Sb_2Te_3 has been reported as the best candidate next to Bi_2Te_3 for room temperature thermoelectric conversion and as the model compound for phase change applications [4]. In both cases, the layered structure is utilized to achieve low thermal conductivity. For Sb_2Te_3 films the influence of stoichiometry, morphology, annealing temperature and crystallinity of the films on thermal conductivity [5] and furthermore on their thermoelectric performance [6,7] have been studied and the most promising results were obtained for near stoichiometric films [8].
Herein, we study the lattice dynamics on an elemental modulated Sb_2Te_3 sample prepared via the nanoalloying method [9,10] by measuring the Sb specific density of phonon states. On the same sample, we identified diffuse x-ray scattering which indicates that even in the as grown state finite correlation length in the basal plane exists.

2 Experimental details

2.1 Sample preparation and thermal conductivity

Repeating layers of the elements Sb and Te with 0.2 nm thickness were deposited on 10 x 10 mm pieces of commercially available $SiO_2(100\text{ nm})/Si$ $(1\,0\,0)$ substrates in an MBE system at room temperature, see Ref. [10]. All layers were deposited to maintain the stoichiometric $40/60$

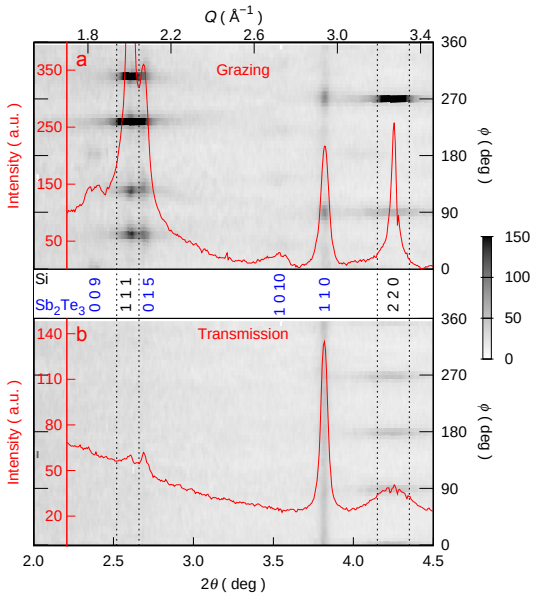

Figure 1 X-ray diffraction pattern by the elemental modulated Sb_2Te_3 film obtained at 295 K using synchrotron radiation in two orientations, see text, (a) grazing incidence geometry and (b) transmission geometry. The background shows the actual detector pattern transformed in $(2\theta,\phi)$ representation and the red lines show the related diffractograms. The expected peak positions of both the Si substrate and the Sb_2Te_3 film are indicated by the Miller indices in the cubic and pseudohexagonal setting, respectively.

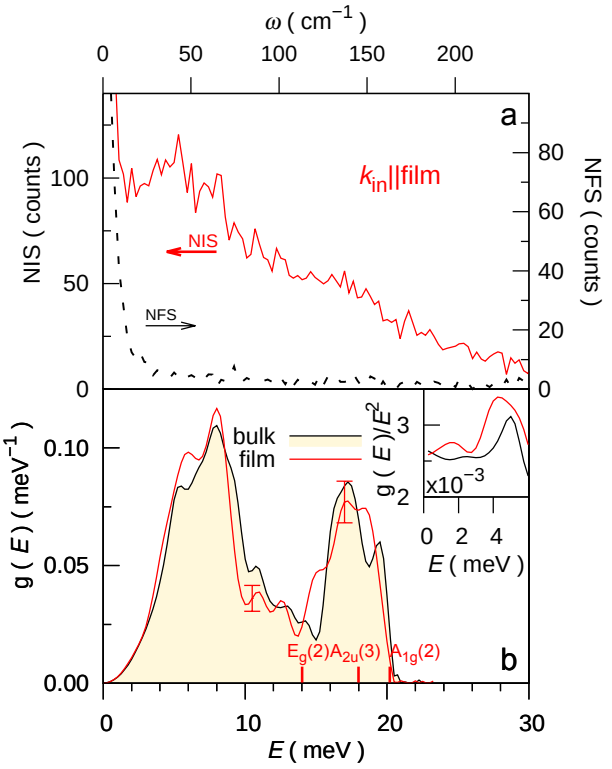

Figure 2 (a) The nuclear inelastic scattering spectrum (red line) and the instrumental function, NFS, (black dashed lines), obtained in the elemental modulated Sb_2Te_3 film with the incident wavevector k_{in} parallel to the film surface. (b) The Sb specific density of phonon states extracted with k_{in} parallel to the surface of an elemental modulated Sb_2Te_3 film (red line) and on bulk polycrystalline Sb_2Te_3 (black line). Inset: The Debye level calculated from the Sb specific DPS measured in Sb_2Te_3.

ratio for Sb/Te given the repeating quintuple pattern. The nominal total thickness of the thin films was 1 μm. The nanoalloyed films are very smooth compared to the epitaxial thin films which tend to exhibit a significant roughness [11]. The cross plane thermal conductivity at room temperature was measured on an as-grown sample using a time domain thermal reflectance measurement system [12,13] calibrated to Si/SiO_2 standard. The results on the annealed samples were reported elsewhere [10].

2.2 Crystallinity and phase purity To verify crystallinity and phase purity, diffraction using synchrotron radiation was carried out at 295 K at 6-ID-D station of the Advanced Photon Source on the Sb_2Te_3 films in two orientations, (i) with the incident, k_{in}, vector parallel to the Si (1 0 0), called transmission geometry and (ii) with k_{in} perpendicular to the Si (1 0 0), called grazing incidence geometry. The wavelength of the measurement was set to 0.142519 Å. Data were collected using an amorphous Si area detector of 2048 x 2048 pixels (pixel size: 200 μm). A sample-detector distance of 1715.5 mm was refined by using diffraction from NIST Si 470c. Both detector patterns are interpeted as follows: the radial distance from the beam center corresponds to the scattering angle 2θ and the circular angle at certain radius corresponds to the azimuthal angle ϕ. The raw data were treated using FIT2D [14] and the detector patterns in azimuthal coordinates, ϕ and 2θ, are shown in Fig. 1. The diffractograms were extracted after integrating intensities at all ϕ for certain 2θ and are superimposed to the detector patterns in Fig. 1.

2.3 Lattice dynamics The lattice dynamics were investigated by means of ^{121}Sb Nuclear Inelastic Scattering [15], NIS, using a backscattering monochromator [16] with a resolution of 1.3 meV for the ^{121}Sb resonance at 37.13 keV. The natural abundance of ^{121}Sb is 57% and no further enrichment is required. The spectra were recorded in 16-bunch mode at the nuclear resonance station ID18 [17] of the European Synchrotron Radiation Facility on the same sample and orientation where diffraction patterns were acquired. In order to minimise multiphonon contributions the measurements were performed at 40 K. The ^{125}Te DPS has not been measured because the samples are too thin to be probed without further isotopic enrichment.

Table 1 Summary of the reflection positions extracted from x-ray diffraction by a nanoalloyed Sb_2Te_3 film in [a]grazing incidence geometry, [b]transmission geometry and comparison with bulk Sb_2Te_3. The FWHM and the reflection positions in the nanoalloyed film were extracted after fiting the data with a lorentzian profile. The reflection positions in bulk Sb_2Te_3 are calculated from Ref. [18] using a wavelength of 0.142519Å. The difference in the interplane distance are calculated using the relation $\delta d = (d_{\text{film}} - d_{\text{bulk}})/d_{\text{bulk}}$. The correlation length, ξ, is also given, see text.

	2θ(deg)				
Reflection	Sb_2Te_3	film	δd, %	FWHM, Å^{-1}	ξ, Å
$(0\,0\,9)$[a]	2.413	2.3 (2)	4.9(4)	0.15 (5)	13(4)
$(0\,1\,5)$[a]	2.586	2.69 (1)	-3.8(1)	0.05 (1)	42(6)
$(1\,0\,10)$[a]	3.476	3.51 (2)	-1.0(1)	0.2 (1)	10(8)
$(1\,1\,0)$[a]	3.815	3.82 (2)	-0.1(1)	0.043 (5)	50(4)
$(1\,1\,0)$[b]				0.035 (5)	63(5)
Si $(1\,1\,1)$[a]	2.606 (1)		-	0.015 (1)	

The NIS measurements were carried out in the same orientation with the XRD measurements. However, because of the overall small sample thickness the obtained statistics are poor when $k_{\text{in}} \perp$ film (transmission geometry) and not used in this study.

3 Results

3.1 Crystallinity and phase purity X-ray diffraction on the films shows only one homogeneous and broad Debye - Scherrer ring of the $(1\,1\,0)$ type in transmission geometry, see Fig. 1b. In grazing incidence geometry broader but discrete reflections are identified not only for the $(1\,1\,0)$ type of reflections but also for the $(0\,0\,9)$ and the $(1\,0\,10)$. The diffuse scattering related to the $(0\,1\,5)$ type of reflections is aligned with the $(1\,1\,1)$ reflections of the silicon substrate. All reflections were fitted with a Lorentzian profile and the extracted parameters are given in Table 1. The full width at half maximum, FWHM, of the Si $(1\,1\,1)$ reflection is also extracted and indicates the instrumental resolution. It appears that the instrumental resolution is much narrower than the film reflections. An estimate of the correlation length, ξ, can be extracted from the FWHM of the reflections, $FWHM_{ref}$, corrected for the instrumental resolution, $FWHM_{inst}$, using $1/\xi = 0.5\sqrt{FWHM_{ref}^2 - FWHM_{inst}^2}$. The correlation length extracted from all reflections is well below 100 Å, see Table 1. Note that the extracted corrrelation length for the $(0\,0\,9)$ reflection is comparable with the length of one quintuple -[Te(I)-Sb-Te(II)-Sb-Te(I)]- stack which is 10 Å. Thus, although crystalline order is identified, long range crystalline order is not fully established in the elemental modulated films.

An estimate of the interplane distance change, δd, was extracted by comparing the positions of the observed reflections with the nominal reflection positions of crystalline Sb_2Te_3, see Table 1. The crystallographic c-axis related to $(0\,0\,9)$ type of reflections appears elongated by $\sim 5\%$ which indicates somewhat loose packing perpendicular to the basal plane, however, the $(1\,1\,0)$ reflection which has only in-plane components has marginally lower 2θ values compared to the 2θ values in bulk polycrystalline samples. This indicates that the elemental modulated Sb_2Te_3 film have almost the same density in-plane with the crystalline counterpart.

3.2 Lattice dynamics The nuclear inelastic scattering spectrum by ^{121}Sb in bulk Sb_2Te_3 has been reported earlier [19]. In this study, we used the same instrumental setup [16] and we obtained the ^{121}Sb nuclear inelastic scattering spectra and the instrumental function, $i.e.$ elastic line, in elemental modulated Sb_2Te_3 films. The elastic line was subtracted and the data were further treated using a modified version [20] of the program DOS [21]. The self consistency of the procedure was confirmed by applying the conventional sum rules [22]. The raw data for the $k_{in} \parallel$ film case are shown in Fig. 2a. The ^{121}Sb specific DPS, $g(E)$, extracted from Fig. 2a is depicted in Fig. 2b. The ^{121}Sb specific DPS shown in Fig. 2b is in excellent agreement with the corresponding obtained on the bulk polycrystalline counterpart [19], which is also shown in the same figure.

The Lamb Mössbauer factor was extracted both from the DPS and the raw spectra. The extracted Sb specific f_{LM} on elemental modulated Sb_2Te_3 at 40 K is $0.18(5)$. In the Debye approximation by using a Debye temperature of 135 K [19] the Sb f_{LM} in Sb_2Te_3 decreases to 0.30 at 40 K. Hence, the f_{LM} on elemental modulated films at 40 K decreases by 0.12 with respect to the bulk counterpart. Such behaviour has been identified also earlier [23] in similar systems.

The mean interatomic force constant is obtained from the second moment of the DPS. The extracted Sb specific mean force constant in the elemental modulated films is, 52(2) N/m, in good aggrement with the corresponding value in the bulk polycrystalline samples, 55(2) N/m [19]. In the Debye representation, both crystalline and elemental modulated Sb_2Te_3 follow almost the same behaviour. The Debye level, $\lim_{E\to 0} \frac{g(E)}{E^2}$, slightly increases in the elemental modulated Sb_2Te_3 structure with respect to crystalline Sb_2Te_3, see inset to Fig. 2b. The average speed of sound, v_s, is extracted from the ^{121}Sb Debye level using

$\lim_{E\to 0}\frac{g(E)}{E^2} = \frac{m_R}{2\pi\hbar^3\rho v_s^3}$, where m_R is the mass of the resonant nucleus and ρ is the mass density. The extracted average speed of sound using a 5% mass density decrease with respect to the bulk value, 6.48g/cm^3, is $1.74(2)$ km/s.

4 Discussion Constant in-plane distances with simultaneous extension of the out-of-plane pseudo-lattice parameter is a characteristic of elemental modulated films obtained by nanoalloying. The ratio of interlayer to intralayer spacing is thus a rough measure of the layer-like character of the system. The higher this ratio is, the weaker the expected layer-layer coupling relative to intralayer bond becomes. Sb_2Te_3 qualifies as a layered crystal. In this study the layer-like character of the elemental modulated films is further enhanced since the interlayer distance is found elongated by $\sim 5\%$ with respect to the crystalline Sb_2Te_3.

The preservation of the elemental modulated pattern is proven by the diffraction patterns shown in Ref. [10]. It is also confirmed in this work not only by the limited correlation length but also by the reduction in the Sb $f_{\rm LM}$. In glasses, the $f_{\rm LM}$ appears reduced mainly due to lower elastic moduli and lower mass density compared to the crystalline counterparts [24]. However, such elemental modulated compounds do not possess all properties of glasses since periodicity at least in one orientation exists, i.e., along the c-axis.

Phonon modes at Γ point in bulk crystalline Sb_2Te_3 were calculated from first principles [25]. The IR active $A_{2u}(3)$ mode at 18 meV, and the Raman active $A_{1g}(2)$ mode at 20 meV, correspond predominantly to Sb displacement along the c-axis. The intraplane vibrational mode at 14 meV is the mixed Sb-Te Raman active mode.

A clear peak in the measured DPS is not shown neither for the IR nor for the Raman active modes. This could be reasonably explained for the $E_g(2)$ mode by the fact that the weighting of the mode at Γ point is not significant compared to the rest of the Brillouin zone. The $A_{2u}(3)$ and the $A_{1g}(2)$ correspond to displacements along the c-axis. However, because the measurement was carried out with the k_{in} normal to the c-axis such a mode will not appear in the measured DPS, see Ref. [26]. A similar effect is observed for Te NIS measurements obtained along and perpendicular to the c-axis of a Bi_2Te_3 single crystal [19]. Otherwise, the extracted Sb specific DPS when $k_{in}\|$film in elemental modulated Sb_2Te_3 films does not change significantly from its bulk counterpart.

The extracted speed of sound practically coincides in bulk samples and elemental modulated films. This is related to a combination of the reduced mass density and the increased Debye level in the elemental modulated film with respect to the bulk counterpart. Similarly only a slight decrease is observed in the acoustic cut-off energy, i.e., the highest energy of the acoustic modes, from 9 meV to 8.5 meV, see Fig.2. This might indicate that once the layered structure is formed, even before the crystallization is fully established, the main features in the DPS already emerge. In case the crystallisation evolves misleading results related to preferred orientation might appear in anisotropic structures.

To quantify the microscopic observations in functional properties an estimate of the macroscopically measured thermal conductivity might be given using the relation extracted by Slack [27], $\kappa_{\rm L} = {\rm A}\frac{\overline{M}\theta_{\rm a}^3 V_{at}^{1/3} N^{1/3}}{\gamma^2 T}$, where $\overline{M}$ is the average atomic mass, $\theta_{\rm a}$ is the acoustic mode Debye temperature which is extracted from the acoustic cut-off energy, N is the number of atoms per primitive cell, $V_{\rm at}$ is the volume per atom, γ is the Grüneisen constant, T is the temperature and $A{\approx}3.1{\cdot}10^{-6}$ is a collection of physical constants. Because the measured DPS on the elemental modulated film is almost identical to the polycrystalline counterpart the vibrational energy defined by the Grüneisen parameter, $\gamma = -\frac{d\ln E}{d\ln V}$, might safely be assumed to be the same in both compounds, $\gamma = 1.7$ [19]. The 5% increase of the volume per atom $V_{\rm at}$, which is related to the corresponding decrease in the mass density in the elemental modulated film, does not increase $\kappa_{\rm L}$ by more than 1% in the film. However, the marginal decrease of the acoustic cut-off energy in the film with respect to the bulk counterpart suggests that the lattice thermal conductivity in the films can be reduced by a maximum of 10% with respect to the bulk. The macroscopically measured cross-plane thermal conductivity on a similar sample is $0.41(4)$ W/m/K. The observed reduction in thermal conductivity by 83% from the bulk value, 2.4 W/m/K, at RT [28] thus appears to be attributed in great extent to the electronic part of the thermal conductivity. Notably, the electrical conductivity in this sample, 164 S/cm, is reduced by 91% compared to the electrical conductivity, 1933 S/cm, of a similar annealed sample [10].

5 Conclusions We show that detailed microscopic lattice dynamical characterization on elemental modulated structures can be achieved by nuclear inelastic scattering. The correlation length of the elemental modulated films was extracted in the as grown state and was found to be finite but less than 100 Å. The main features in the density of phonon states in polycrystalline Sb_2Te_3 and elemental modulated films of the same stoichiometry seem to be strongly related to the layered pattern of the crystallographic structure. The extracted speed of sound is practically the same mainly due to the combination of a reduced mass density and an increased Debye level. Thus, the reduction in the macroscopically measured thermal conductivity appears to be attributed to a great extent in the electronic part of the thermal conductivity.

Acknowledgements The DFG priority program SPP1386 'Nanostructured Thermoelectrics' and the Helmholtz – University Young Investigator Group 'Lattice Dynamics in Emerging Functional Materials' are acknowledged for the financial support of this study. RH and DB acknowledge the European Synchrotron Radiation Facility and the Advanced Photon Source for provision

of synchrotron radiation beam time and the helpful discussions with Dr. A. Chumakov and Dr. R. Rüffer at ID-18 and the help of Dr. D. Robinson during data acquisition at 6-ID-D, respectively.

References

[1] Makovicky, E. *Rev. Mineral. Geochem. 61*, 7 (**2006**)
[2] Schmid, P. *Festkörperprobleme 16*; Advances in Solid State Physics Vol. 16; pp 47–64 (**1976**)
[3] Zallen, R.; Slade, M. *Phys. Rev. B 9*, 1627 (**1974**)
[4] Lencer, D.; Salinga, M.; Grabowski, B.; Hickel, T.; Neugebauer, J.; Wuttig, M. *Nat. Mater. 7*, 971 (**2008**)
[5] Fan, X. A.; Yang, J. Y.; Xie, Z.; Li, K.; Zhu, W.; Duan, X. K.; Xiao, C. J.; Zhang, Q. Q. *J. Phys. D.: Appl. Phys. 40*, 5975 (**2007**)
[6] Li, S.; Soliman, H. M. A.; Zhou, J.; Toprak, M. S.; Muhammed, M.; Platzek, D.; Ziolkowski, P.; Müller, E. *Chem. Mater. 20*, 4403 (**2008**)
[7] Harris, F. R.; Standridge, S.; Feik, C.; Johnson, D. *Angew. Chem. Int. Engl 42*, 5295 (**2003**)
[8] Kim, Y.; Di Venere, A.; Wong, G. K. L.; Ketterson, J. B.; Cho, S.; Meyer, J. R. *J. Appl. Phys. 91*, 715 (**2002**)
[9] Johnson, D. C. *Curr. Opin. Solid. St. M. 3*, 159 (**1998**)
[10] Winkler, M.; Liu, X.; Konig, J. D.; Buller, S.; Schurmann, U.; Kienle, L.; Bensch, W.; Bottner, H. *J. Mater. Chem. 22*, 11323 (**2012**)
[11] Nurnus, J. *PhD thesis*; Fakültat für Physik der Albert-Ludwigs-Universität Freiburg i. Br., Germany, (**2001**)
[12] Christescu, C.; Cahill, D. G.; Heideman, C.; Lin, Q.; Mortensen, C.; Johnson, D.; Rostek, R.; Böttner, H. *J. Appl. Phys. 104*, 033533 (**2008**)
[13] Cahill, D. G. *Rev. Sci. Instr. 75*, 5119 (**2004**)
[14] Hammersley, A. P.; Svensson, S. O.; Hanfland, M.; Fitch, A. N.; Hausermann, D. *High Pressure Res. 14*, 235 (**1996**)
[15] Wille, H.-C.; Hermann, R. P.; Sergueev, I.; Pelzer, U.; Möchel, A.; Claudio, T.; Perßon, J.; Rüffer, R.; Said, A.; Shvyd'ko, Y. V. *Europhys. Lett. 91*, 62001 (**2010**)
[16] Sergueev, I.; Wille, H.-C.; Hermann, R. P.; Bessas, D.; Shvyd'ko, Y. V.; Zajac, M.; Rüffer, R. *J. Synchrotron Radiat. 18*, 802 (**2011**)
[17] Rüffer, R.; Chumakov, A. *Hyperfine Interact. 97-98*, 589 (**1996**)
[18] Anderson, T. L.; Krause, H. *Acta Crystallogr., Sect. B: Struct. Sci 30*, 1307 (**1974**)
[19] Bessas, D.; Sergueev, I.; Wille, H.-C.; Persson, J.; Ebling, D.; Hermann, R. *Phys. Rev. B 86*, 224301 (**2012**)
[20] The DOS program was modified for reconvoluting the extracted DPS with a gaussian function with the same FWHM as the measured time integrated NFS
[21] Kohn, V.; Chumakov, A. *Hyperfine Interact. 125*, 205 (**2000**)
[22] Lipkin, H. J. *Phys. Rev. B 52*, 10073 (**1995**)
[23] Boolchand, P.; Bresser, W.; Zhang, M.; Wu, Y.; Wells, J.; Enzweiler, R. *J. Non-Cryst. Solids 182*, 143 (**1995**)
[24] Bass, J. D. *Elasticity of minerals, glasses and melts, in mineral physics and crystallography*; American Geophysical Union (**1995**)
[25] Sosso, G. C.; Caravati, S.; Bernasconi, M. *J. Phys. Condens. Matter 21*, 095410 (**2009**)
[26] Chumakov, A. I.; Rüffer, R.; Baron, A. Q. R.; Grünsteudel, H.; Grünsteudel, H. F.; Kohn, V. G. *Phys. Rev. B 56*, 10758 (**1997**)
[27] Slack, G. A. *Solid State Physics* Academic Press (**1797**)
[28] Spitzer, D. *J. Phys. Chem. Solids 31*, 19 (**1970**)